Editors' Suggestion | Featured in Physics

Phonon Magnetochiral Effect

T. Nomura,[1,*] X.-X. Zhang,[2,3,*] S. Zherlitsyn,[1] J. Wosnitza,[1,4] Y. Tokura,[2,5] N. Nagaosa,[2,5] and S. Seki[2,5,6]
[1]*Hochfeld-Magnetlabor Dresden (HLD-EMFL), Helmholtz-Zentrum Dresden-Rossendorf, 01328 Dresden, Germany*
[2]*Department of Applied Physics, The University of Tokyo, Tokyo 113-8656, Japan*
[3]*Quantum Matter Institute, University of British Columbia, Vancouver BC V6T 1Z4, Canada*
[4]*Institut für Festkörper-und Materialphysik, TU-Dresden, 01062 Dresden, Germany*
[5]*RIKEN Center for Emergent Matter Science (CEMS), Wako 351-0198, Japan*
[6]*Institute of Engineering Innovation, The University of Tokyo, Tokyo 113-8656, Japan*

(Received 26 September 2018; published 10 April 2019)

The magnetochiral effect (MCE) of phonons, a nonreciprocal acoustic propagation arising due to symmetry principles, is demonstrated in the chiral-lattice ferrimagnet Cu_2OSeO_3. Our high-resolution ultrasound experiments reveal that the sound velocity differs for parallel and antiparallel propagation with respect to the external magnetic field. The sign of the nonreciprocity depends on the chirality of the crystal in accordance with the selection rule of the MCE. The nonreciprocity is enhanced below the magnetic ordering temperature and at higher ultrasound frequencies, which is quantitatively explained by a proposed magnon-phonon hybridization mechanism.

DOI: 10.1103/PhysRevLett.122.145901

There are physical phenomena that arise due to the fundamental symmetry principles; mirror symmetry breaking in chiral matters leads to natural optical or acoustic activity and time-reversal symmetry breaking by magnetic fields leads to magnetic optical or acoustic activity. When both symmetries are simultaneously broken, a nonreciprocal property appears, the so-called magnetochiral effect (MCE). The MCE has been observed for photons [1–5], electrons [6–9], and magnons [10–12]. Here, the (quasi) particles with the propagation vector $\mathbf{k}$ parallel and antiparallel to the magnetic field $\mathbf{H}$ show different propagation properties. Owing to the symmetry origin of the MCE (time-reversal and mirror symmetry breakings), any changes in the sign of $\mathbf{H}$ or the chirality of the crystals ($\sigma = \pm 1$) result in a reversed nonreciprocity for $\pm\mathbf{k}$.

From the symmetry consideration, the MCE should exist also for phonons (elementary vibrations of a crystal lattice) [13,14], which has not been observed experimentally. A phonon is one of the most ubiquitous quasiparticle, responsible for the heat and sound transmissions in solids. The nonreciprocal phonons could enable the rectifications of the heat and sound, which are attractive for phononics applications [15–18]. However, nonreciprocal flows of heat and sound have been realized only in artificial structures [19–22] or for surface-acoustic waves [23,24]. The MCE of phonons, which realizes the nonreciprocal thermal and acoustic flows in bulk media, is a promising strategy for future technologies. Furthermore, confirming the universality of the MCE for the representative (quasi)particles (photon, electron, magnon, and phonon) will be an important milestone for fundamental science. Herein, we have revealed the last missing piece of them, the phonon MCE, with high-resolution ultrasound measurements on Cu_2OSeO_3.

Our target compound Cu_2OSeO_3 possesses a chiral cubic crystal structure with space group $P2_13$, as shown in Fig. 1. Both left-handed (L, $\sigma = -1$) and right-handed (D, $\sigma = +1$) single crystals can be obtained, which are distinguishable by natural optical activity measurements. This compound contains two inequivalent Cu^{2+} ($S = 1/2$) sites with a ratio of 3:1. As a result, a local ferrimagnetic spin arrangement with three-up-one-down manner is stabilized below $T_C \approx 58$ K [25]. The Dzyaloshinskii-Moriya (DM) interaction causes an additional long-period

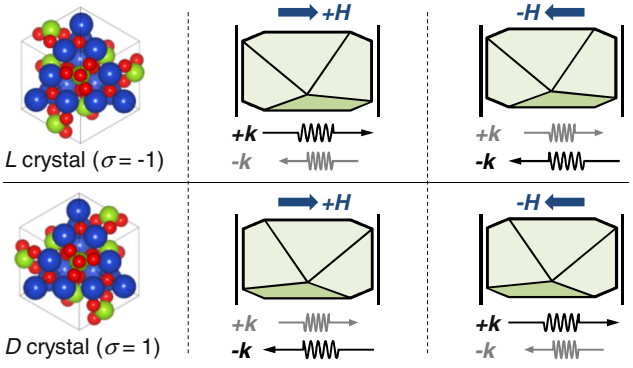

FIG. 1. Experimental configurations to examine the phonon MCE. Chirality of the crystal ($\sigma = \pm 1$), sound propagation direction ($\pm\mathbf{k}$), and magnetic field direction ($\pm\mathbf{H}$) are successively inverted and the relative sound velocities are compared. The L- and D-type crystal structures of Cu_2OSeO_3 are shown along the [111] direction, where the spheres represent Cu (blue), O (red), and Se (green) atoms.

($\lambda \approx 62$ nm) helical spin modulation at $H = 0$, and external magnetic fields induce successive magnetic phase transitions from helical to conical and to collinear magnetic configurations [26]. Because of the interplay between the chiral crystal symmetry and magnetism, various exciting properties such as magnetic skyrmions [26–28], multiferroicity [25,27–29], and magnon MCE [10] have been reported. Therefore, Cu_2OSeO_3 is an ideal candidate to observe the phonon MCE.

The high-resolution sound-velocity measurements are based on the ultrasonic pulse-echo technique with a phase-sensitive detection. Two $LiNbO_3$ transducers were attached on the polished surfaces of the homochiral single crystals of Cu_2OSeO_3 for excitation or detection. The relative changes of the sound velocity $\Delta v/v_0$ for L- and D-type crystals ($\sigma = \pm 1$) were measured with $\pm\mathbf{k}$ and $\pm\mathbf{H}$ geometries to examine the MCE (Fig. 1). The results are compared for the different acoustic modes, ultrasound frequencies ($\omega/2\pi$), and temperatures (T). In this research, two pairs of L and D crystals were investigated to confirm the reproducibility. For experimental details and the results for another pair of crystals with the experimental configuration $\mathbf{k}\|[111]$, see the Supplemental Material [30].

Figure 2(a) shows the results for the transverse acoustic (TA, with displacement vector $\mathbf{u}\perp\mathbf{k}$) mode in the L crystal measured in Faraday geometry ($\mathbf{H}\|\mathbf{k}$) at 2 K. Magnetic phase transitions from helical to conical ($H_{c1} = 30$ mT) and from conical to collinear ($H_{c2} = 95$ mT) states are observed as a step and a minimum in $\Delta v/v_0$, respectively (see also Ref. [38]). Remarkably, $\Delta v/v_0$ slightly differs at H_{c2} for $\pm\mathbf{k}$, which is a clear feature of the nonreciprocity. When the magnetic field is reversed, the sign of the observed nonreciprocity becomes opposite. For a crystal with opposite chirality [D type, Fig. 2(b)], all these nonreciprocal relations are reversed. Therefore, the nonreciprocity is reversed for any changes in sign of σ, $\mathbf{k}$, and $\mathbf{H}$. Such a nonreciprocity disappears in Voigt geometry ($\mathbf{k}\perp\mathbf{H}$) for the same TA mode (Fig. S2 in the Supplemental Material [30]). These selection rules evidence that the observed nonreciprocity originates from the phonon MCE. Interestingly, the magnitude of the MCE for the longitudinal acoustic (LA, with $\mathbf{u}\|\mathbf{k}\|\mathbf{H}$) mode is much smaller [Fig. 2(c)] and cannot be identified within the experimental resolution of $\Delta v/v_0 \approx 10^{-6}$.

For further analysis on the MCE of the TA mode, we plotted $\Delta v/v_0$ as a function of $|H|$ in Fig. 2(d). Here, we introduce the degree of the MCE as

$$g_{\mathrm{MC}}(H) = \frac{\Delta v(+\mathbf{H})}{v_0} - \frac{\Delta v(-\mathbf{H})}{v_0} = \frac{v(+\mathbf{H}) - v(-\mathbf{H})}{v_0}. \quad (1)$$

As shown in Fig. 2(e), the nonreciprocity is dramatically enhanced upon the transition into the collinear spin state (H_{c2}) and rapidly weakens at higher fields. Figure 2(f) shows the maximum magnitude of the MCE $g_{\mathrm{MC}}(H_{c2})$ as a function of ultrasound frequency. The MCE is enhanced nonlinearly towards higher frequencies.

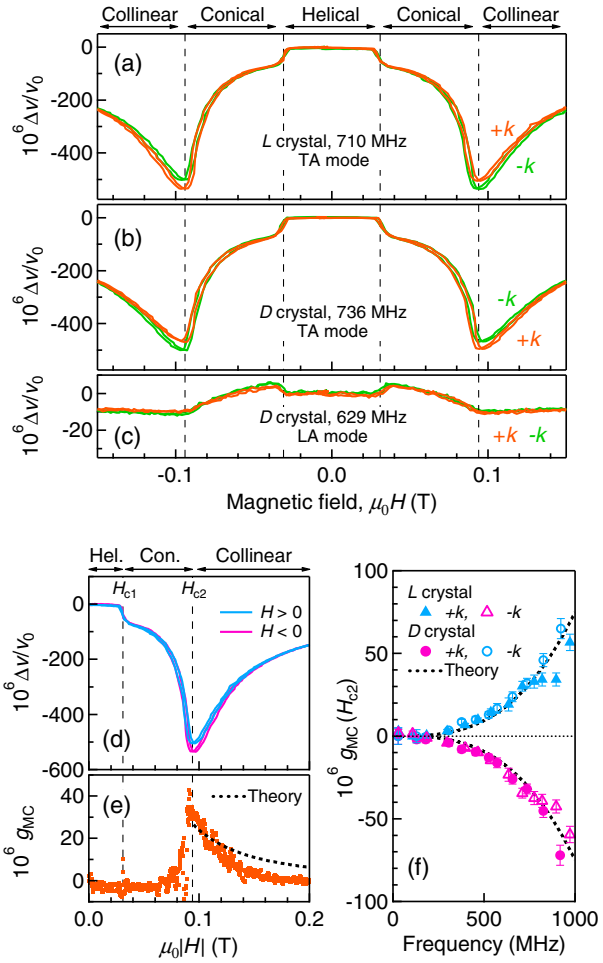

FIG. 2. (a)–(c) Relative changes of the sound velocity $\Delta v/v_0$ as a function of magnetic field H at 2 K. The transverse $(c_{11} - c_{12})/2$ mode ($\mathbf{k}\|\mathbf{H}\|[110]$, $\mathbf{u}\|[1\bar{1}0]$) for the (a) L and (b) D crystal, and (c) the longitudinal $(c_{11} + c_{12} + 2c_{44})/2$ mode ($\mathbf{k}\|\mathbf{u}\|\mathbf{H}\|[110]$) for the D crystal are presented. The sound propagation direction ($\pm\mathbf{k}$) and the ultrasound frequency are denoted for each curve. All the experimental results are shown for up and down field sweeps. The sound velocities for the transverse and longitudinal modes are $v_{(c_{11}-c_{12})/2} = 2.3$ km/s and $v_{(c_{11}+c_{12}+2c_{44})/2} = 4.1$ km/s, respectively. (d) $\Delta v/v_0$ as a function of $|H|$ for the transverse mode at 710 MHz with $+\mathbf{k}$ in the L crystal. The results for $H > 0$ ($H < 0$) are shown by cyan (magenta). (e) Magnitude of the MCE g_{MC} as a function of $|H|$, which corresponds to the difference between the data for $+H$ and $-H$ in Fig. 2(d). (f) Maximum magnitude of the MCE $g_{\mathrm{MC}}(H_{c2})$ at 2 K as a function of ultrasound frequency for the transverse mode. The results are shown for $\sigma = \pm 1$ and $\pm\mathbf{k}$. The black dotted curves [Figs. 2(e) and 2(f)] denote the calculated results based on Eq. (2) with the magnetoelastic coupling constant $\gamma = 90$.

T dependence of $g_{\mathrm{MC}}(H_{c2})$ is shown in Fig. 3(a). The MCE weakens at higher T and linearly vanishes with

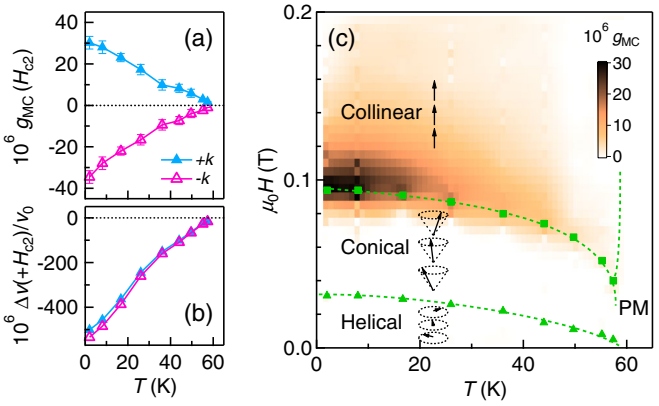

FIG. 3. Temperature dependencies of (a) $g_{\mathrm{MC}}(H_{c2})$ and of (b) the relative change of the sound velocity at H_{c2} for the transverse mode. (c) Contour plot of g_{MC} mapped on the T-H phase diagram. The phase boundaries are determined by the anomalies in $\Delta v/v_0$ (triangles and squares). Here, the results for the L crystal at 710 MHz are used.

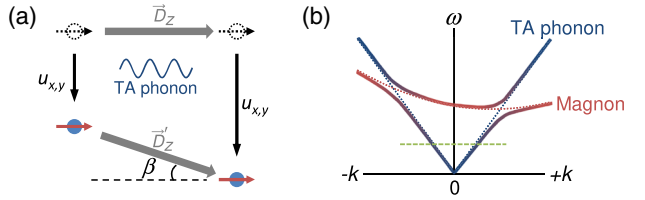

FIG. 4. (a) Magnetoelastic coupling due to the shear strain. TA phonons cause the displacements $u_{x,y}$ of the neighboring lattice sites (blue circles) from the original places (dotted circles). The original DM vector $\vec{D}_z$ is modified to $\vec{D}'_z$ by a tilting angle β. The magnetic moments (dashed and red arrows) and the TA phonon propagation are along the $\hat{z}$ direction. In reality, the two displacements are not necessarily in the same direction. (b) Dispersions of the magnon and phonon bands hybridized by the chiral magnetoelastic coupling. The original dispersions are shown by dotted lines. One of the circularly polarized phonon mode hybridizes with the magnons, leading to the anticrossing. Another mode does not hybridize and its dispersion remains as the original blue dotted line. The ultrasound frequency used in this study (dashed line) was always lower than the hybridization frequency.

approaching $T_{\mathrm{C}} \approx 58$ K. With increasing T, the relative change of the sound velocity itself also decreases [Fig. 3(b)]. For an overview, the contour plot of g_{MC} is mapped on the T-H phase diagram [Fig. 3(c)]. Obviously, the presence of nonreciprocity is related to the underlying spin structure. The MCE is absent in the helical and conical spin states, and g_{MC} takes maximum magnitude at near H_{c2} in the collinear spin state.

When considering the mechanism of the phonon MCE, there are three important features. First, the MCE appears at H_{c2} and rapidly weakens at higher fields [Fig. 2(e)]. The absence of the MCE below H_{c2} (helical and conical states) is observed also for the magnons in Cu_2OSeO_3, where the DM interaction causes the asymmetric magnon dispersion in the collinear spin state but such an asymmetry between $\pm\mathbf{k}$ is lost by the folding back of magnon branch in the helical or conical spin states [10,39]. This common feature indicates a correlation between the MCEs of magnons and phonons. Second, the MCE is dramatically enhanced at higher ultrasound frequencies [Fig. 2(f)]. In our experiment, the phase velocity of acoustic phonons $v = \omega/k$ is measured. Ultrasound frequencies of a few hundreds MHz are rather close to the Brillouin-zone center where the acoustic phonon dispersion is usually linear. The observed frequency dependence indicates that the MCE is related to the nonlinear dispersion of the acoustic phonons. Third, the magnitude of the MCE and $\Delta v/v_0$ for the LA mode are much smaller than the TA mode [Figs. 2(a)–2(c)]. This implies that the shear strain connected with the TA phonon plays a dominant role in the observed MCE.

The underlying picture is that the acoustic phonons inherit the nonreciprocity from the asymmetric magnon excitations via a magnon-phonon band hybridization [Fig. 4(b)]. This magnon-phonon hybridization results in a band repulsion or anticrossing, which deforms the linear dispersion of the TA phonons. When the magnon dispersion possesses an asymmetry due to the DM interaction [10,39], the hybridization points differ for $\pm\mathbf{k}$ and the acoustic phonons acquire the nonreciprocity. When the ultrasound frequency is close to the hybridization points, the MCE is dramatically enhanced. Besides, the magnitude of the MCE depends on the degree of the anticrossing produced by the magnetoelastic coupling.

For the origin of the magnon-phonon hybridization, we propose a chiral magnetoelastic coupling due to the modulation of the DM interaction by shear strains. The major effect of TA phonons is to tilt the bonds and to modify the DM interaction, in contrast to the elongation or compression due to LA phonons [40,41]. We base the discussion on the minimal magnetic Hamiltonian $\mathcal{H}_{\mathrm{latt}} = \sum_{\vec{r},\hat{\alpha}}[-J\vec{S}_{\vec{r}} \cdot \vec{S}_{\vec{r}+\hat{\alpha}} - \vec{D}_\alpha \cdot \vec{S}_{\vec{r}} \times \vec{S}_{\vec{r}+\hat{\alpha}} - g\vec{S}_{\vec{r}} \cdot \vec{B}]$, including the nearest-neighbor exchange interaction J, the DM interaction D, and the Zeeman energy, in which $g = 2\mu_{\mathrm{B}}$ and $\vec{D}_\alpha$ denotes the DM vector on the bond along the $\hat{\alpha}$ direction. The collinear phase is treated as an effective ferromagnetic state averaged over the unit cell. We take into account spin waves, i.e., fluctuations $\delta\vec{S}$ in this ordered phase, coupled with phonons propagating along the direction $\hat{z}\|\mathbf{H}$. Crucially, the leading-order effect should result from the harmonic magnetoelastic coupling, i.e., bilinear in both the spin-wave and phonon coordinates. As can be seen from the form of $\mathcal{H}_{\mathrm{latt}}$, the desired coupling must come from the DM interaction because the spin-wave fluctuations of the exchange term are always quadratic in $\delta\vec{S}\perp\hat{z}$ in this state with ordered moment $\langle S^z\rangle$. Most importantly, for the acoustic wave propagating parallel to $\hat{z}$, only the TA phonon can generate bilinear couplings through modifying $\vec{D}_z$ while the LA phonon leads to higher order effects,

e.g., two-magnon processes due to couplings quadratic in the transverse spin moments. This favorably explains the observed (ir)relevance of TA (LA) phonons.

As shown in Fig. 4(a), the TA phonon displacement $\vec{u} = (u_x, u_y)$ changes the DM vector to $\vec{D}_z{}' = D\hat{z} + \gamma D \partial_z u_i \hat{i}$ by a small angle $\beta = \partial_z |\vec{u}|$. Here, we introduce a phenomenological dimensionless magnetoelastic coupling constant γ since the tilting induced by TA phonons is a lattice shear strain rather than merely a rotation of the bonds. Then, one can arrive at the Lagrangian density describing the chiral bilinear interaction $\mathcal{L}_{\rm me} = \gamma D \langle S^z \rangle (-\partial_z u_x \partial_z S^y + \partial_z u_y \partial_z S^x)$ [30]. This unique harmonic coupling proportional to the ordered moment $\langle S^z \rangle$ yields observable effects only quadratic in $\langle S^z \rangle$ as understood via a second-order perturbation. The ordered moment $\langle S^z \rangle$ and hence the experimentally detected responses are suppressed when T increases. This particularly corroborates with the roughly linear T dependencies of both $g_{\rm MC}$ and $\Delta v / v_0(H_{c2})$ as shown in Figs. 3(a) and 3(b) since $\langle S^z \rangle$ scales as $\sqrt{|T - T_{\rm C}|}$ near the magnetic phase transition.

This chiral coupling lifts the degeneracy in the pure phonon theory and makes two nondegenerate eigenstates of the left- and right-circularly polarized (LCP and RCP) TA phonon modes. Here, only one phonon branch selectively hybridizes with magnons [Fig. 4(b)] since only right-handed polarization exists for ferromagnetic-type spin waves with respect to the magnetization, which is different from the case in antiferromagnets [42]. Experimentally, as a linearly polarized sound wave is injected and detected, a superposition of the intact and the hybridized circularly polarized waves results in an acoustic beat typically of the form $2 \sin[(k^u + k^a/2)z + \omega t] \cos[(k^u - k^a/2)z]$, where $k^{a(u)}$ is the wave number (un)affected by the hybridization at the ultrasound frequency. Here, the beating envelope variation is negligibly small within the 2 mm sample thickness (see the Supplemental Material [30]). Therefore, one experimentally detects half the nonreciprocity that occurs for the hybridized phonons.

On the basis of these understandings, one can readily construct a solvable magnon-phonon interacting theory. Deriving an effective theory of the phonon, one is able to directly calculate the sound-velocity change $\Delta v / v_0 = -(\gamma^2 \langle S^z \rangle^2 S D^2 k^2 / a_0 c \Delta_B)$ and the magnitude of the MCE

$$g_{\rm MC} = \frac{4\gamma^2 \langle S^z \rangle^2 S^2 D^3 k^3}{c \Delta_B^2}, \tag{2}$$

in which a_0, S, c, Δ_B are the lattice constant, the total spin moment, the elastic constant, and the spin-wave gap, respectively (see the Supplemental Material for details [30]). This expression suggests that the MCE is enhanced at higher ultrasound frequencies ($k \propto \omega$) and at H_{c2} where the soft-mode magnon band hybridizes with the phonon band at rather low frequencies ($\Delta_B \approx 3$ GHz) [10]. The experimental results are compared with Eq. (2); the theoretically expected $g_{\rm MC} \propto \omega^3$ relationship agrees well with the observed frequency dependence [Fig. 2(f)], and the H dependence of $g_{\rm MC}$ is also reproduced qualitatively [Fig. 2(e)]. The slight quantitative deviation might occur because the magnon-phonon hybridization point is too far from the Brillouin-zone center at higher H. In the theoretical derivations, magnon and phonon dispersions are approximated to be linear in k; however at larger k, nonlinear dispersions become more relevant. Nevertheless, the overall agreement between the theory and experiment, i.e., the significance of TA waves and reproduction of T, ω and H dependencies of $g_{\rm MC}$, strongly suggests that the present magnon-phonon hybridization mechanism associated with the nonreciprocal phonon dispersion well captures the essence of the observed phonon MCE.

Note that another form of the spin-phonon coupling given by $a(\partial_z u_x S^z S^x + \partial_z u_y S^z S^y) + b \partial_z u_z (S^z)^2$, which corresponds to a single-spin anisotropy energy induced by phonon displacements, is allowed by symmetry and can even become the leading-order term. However, we do not consider this term due to the following reasons. (i) It is known that modulation of DM interaction induced by strain is very large, both from experiment and theory in other chiral magnets [35,36]. (ii) The acoustic phonon mainly modulates the relative position of the unit cells, and hence should not influence the physical properties determined within the unit cell, e.g., the single-spin anisotropy. (iii) The experimentally observed ω^3 dependence of the asymmetry can be explained by the modulation of the DM interaction, while that of the single-spin anisotropy gives a linear dependence in ω. Therefore, from this experimental fact, we regard the former as the dominant effect, although the latter effect could give a dominant contribution in the small-ω limit.

In conclusion, the nonreciprocal sound propagations are observed in Cu_2OSeO_3, which are due to the phonon MCE. The selection rule of the MCE is confirmed by the complete set of experimental geometries. The magnitude of the MCE as a function of ω, H, and T is well explained by the proposed magnon-phonon hybridization mechanism. While the observed magnitude of MCE remains rather small at this stage, its ω^3 dependence suggests that further enhancement of the effect is possible. In particular, when the excitation frequency is located within one of the hybridization gaps, the unidirectional phonon propagation can be expected for the mode shown in Fig. 4(b). In principle, the phonon MCE can be expected for any chiral-lattice magnets, and the present results suggest a new intrinsic strategy for the nonreciprocal sound or heat transmission based on a single-phase bulk compound.

This work was partly supported by the JSPS KAKENHI Grants-In-Aid for Scientific Research (No. 18H03676, No. 18H03685, No. 17H05186, No. 16J07545, and

No. 26103006), supported by PRESTO (Grant No. JPMJPR18L5) from JST, by the DFG through SFB 1143, and by HLD at HZDR, member of the European Magnetic Field Laboratory. T. N. was supported by the JSPS through a Grant-in-Aid for JSPS Fellows. N. N. was also supported by CREST, Japan Science and Technology (No. JPMJCR16F1), and ImPACT Program of Council for Science, Technology and Innovation (Cabinet office, Government of Japan, 888176) [43].

[*] These two authors contributed equally
[1] G. L. J. A. Rikken and E. Raupach, Nature (London) **390**, 493 (1997).
[2] M. Vallet, R. Ghosh, A. Le Floch, T. Ruchon, F. Bretenaker, and J. Y. Thépot, Phys. Rev. Lett. **87**, 183003 (2001).
[3] C. Koerdt, G. Düchs, and G. L. J. A. Rikken, Phys. Rev. Lett. **91**, 073902 (2003).
[4] C. Train, R. Gheorghe, V. Krstic, L. M. Chamoreau, N. S. Ovanesyan, G. L. J. A. Rikken, M. Gruselle, and M. Verdaguer, Nat. Mater. **7**, 729 (2008).
[5] Y. Okamura, F. Kagawa, S. Seki, M. Kubota, M. Kawasaki, and Y. Tokura, Phys. Rev. Lett. **114**, 197202 (2015).
[6] G. L. J. A. Rikken, J. Fölling, and P. Wyder, Phys. Rev. Lett. **87**, 236602 (2001).
[7] V. Krstic, S. Roth, M. Burghard, K. Kern, and G. L. J. A. Rikken, J. Chem. Phys. **117**, 11315 (2002).
[8] F. Pop, P. Auban-Senzier, E. Canadell, G. L. J. A. Rikken, and N. Avarvari, Nat. Commun. **5**, 3757 (2014).
[9] T. Yokouchi, N. Kanazawa, A. Kikkawa, D. Morikawa, K. Shibata, T. Arima, Y. Taguchi, F. Kagawa, and Y. Tokura, Nat. Commun. **8**, 866 (2017).
[10] S. Seki, Y. Okamura, K. Kondou, K. Shibata, M. Kubota, R. Takagi, F. Kagawa, M. Kawasaki, G. Tatara, Y. Otani, and Y. Tokura, Phys. Rev. B **93**, 235131 (2016).
[11] R. Takagi, D. Morikawa, K. Karube, N. Kanazawa, K. Shibata, G. Tatara, Y. Tokunaga, T. Arima, Y. Taguchi, Y. Tokura, and S. Seki, Phys. Rev. B **95**, 220406(R) (2017).
[12] Y. Iguchi, S. Uemura, K. Ueno, and Y. Onose, Phys. Rev. B **92**, 184419 (2015).
[13] D. Szaller, S. Bordács, and I. Kézsmárki, Phys. Rev. B **87**, 014421 (2013).
[14] Y. Tokura and N. Nagaosa, Nat. Commun. **9**, 3740 (2018).
[15] N. Li, J. Ren, L. Wang, G. Zhang, P. Hänggi, and B. Li, Rev. Mod. Phys. **84**, 1045 (2012).
[16] M. Maldovan, Nature (London) **503**, 209 (2013).
[17] A. D. O'Connell *et al.*, Nature (London) **464**, 697 (2010).
[18] A. Fornieri and F. Giazotto, Nat. Nanotechnol. **12**, 944 (2017).
[19] C. W. Chang, D. Okawa, A. Majumdar, and A. Zettl, Science **314**, 1121 (2006).
[20] B. Liang, X. S. Guo, J. Tu, D. Zhang, and J. C. Cheng, Nat. Mater. **9**, 989 (2010).
[21] R. Fleury, D. L. Sounas, C. F. Sieck, M. R. Haberman, and A. Alú, Science **343**, 516 (2014).
[22] E. Walker, A. Neogi, A. Bozhko, Yu. Zubov, J. Arriaga, H. Heo, J. Ju, and A. A. Krokhin, Phys. Rev. Lett. **120**, 204501 (2018).
[23] J. Heil, B. Lüthi, and P. Thalmeier, Phys. Rev. B **25**, 6515 (R) (1982).
[24] R. Sasaki, Y. Nii, Y. Iguchi, and Y. Onose, Phys. Rev. B **95**, 020407(R) (2017).
[25] J.-W. G. Bos, C. V. Colin, and T. T. M. Palstra, Phys. Rev. B **78**, 094416 (2008).
[26] S. Seki, J.-H. Kim, D. S. Inosov, R. Georgii, B. Keimer, S. Ishiwata, and Y. Tokura, Phys. Rev. B **85**, 220406(R) (2012).
[27] S. Seki, X. Z. Yu, S. Ishiwata, and Y. Tokura, Science **336**, 198 (2012).
[28] J. S. White, K. Prša, P. Huang, A. A. Omrani, I. Živković, M. Bartkowiak, H. Berger, A. Magrez, J. L. Gavilano, G. Nagy, J. Zang, and H. M. Rønnow, Phys. Rev. Lett. **113**, 107203 (2014).
[29] S. Seki, S. Ishiwata, and Y. Tokura, Phys. Rev. B **86**, 060403 (R) (2012).
[30] See Supplemental Material at http://link.aps.org/supplemental/10.1103/PhysRevLett.122.145901 for details of the experiment and theory, which includes Refs. [31–37].
[31] K. H. Miller, X. S. Xu, H. Berger, E. S. Knowles, D. J. Arenas, M. W. Meisel, and D. B. Tanner, Phys. Rev. B **82**, 144107 (2010).
[32] S. Zherlitsyn, S. Yasin, J. Wosnitza, A. A. Zvyagin, A. V. Andreev, and V. Tsurkan, Low Temp. Phys. **40**, 123 (2014).
[33] L. D. Landau and E. M. Lifshitz, *Theory of Elasticity* (Butterworth-Heinemann, Oxford, 1986), 3rd ed.
[34] Y. Onose, Y. Okamura, S. Seki, S. Ishiwata, and Y. Tokura, Phys. Rev. Lett. **109**, 037603 (2012).
[35] T. Koretsune, N. Nagaosa, and R. Arita, Sci. Rep. **5**, 13302 (2015).
[36] K. Shibata *et al.*, Nat. Nanotechnol. **10**, 589 (2015).
[37] T. Schwarze, J. Waizner, M. Garst, A. Bauer, I. Stasinopoulos, H. Berger, C. Pfleiderer, and D. Grundler, Nat. Mater. **14**, 478 (2015).
[38] D. M. Evans, J. A. Schiemer, M. Schmidt, H. Wilhelm, and M. A. Carpenter, Phys. Rev. B **95**, 094426 (2017).
[39] M. Kataoka, J. Phys. Soc. Jpn. **56**, 3635 (1987).
[40] X.-X. Zhang and N. Nagaosa, New J. Phys. **19**, 043012 (2017).
[41] N. Kanazawa, Y. Nii, X.-X. Zhang, A. S. Mishchenko, G. De Filippis, F. Kagawa, Y. Iwasa, N. Nagaosa, and Y. Tokura, Nat. Commun. **7**, 11622 (2016).
[42] J. Lan, W. Yu, and J. Xiao, Nat. Commun. **8**, 178 (2017).
[43] See https://www8.cao.go.jp/cstp/english/panhu/index.html.